

# A Consistent Picture of Electronic Raman Scattering and Infrared Conductivity in the Cuprates

T.P. Devereaux<sup>1\*</sup> and A.P. Kampf<sup>2</sup>

<sup>1</sup> *Department of Physics, The George Washington University, Washington, DC 20052*

<sup>2</sup> *Theoretische Physik III, Elektronische Korrelationen und Magnetismus, Institut für Physik, Universität Augsburg, 86135 Augsburg, Germany*

Calculations are presented for electronic Raman scattering and infrared conductivity in a  $d_{x^2-y^2}$  superconductor including the effects of elastic scattering via anisotropic impurities and inelastic spin-fluctuation scattering. A consistent description of experiments on optimally doped Bi-2212 is made possible by considering the effects of correlations on both inelastic and elastic scattering.

PACS numbers: 74.25.Jb, 71.27.+a, 78.30-j

Impurity effects in the cuprates have played a major role in clarifying the nature of unconventional superconductivity. Via the change in the density of states (DOS) near the Fermi level, crossover behavior of low temperature transport and thermodynamics quantities could be explored as a testing ground for unconventional pairing [1]. Examples include the  $T$  to  $T^2$  crossover in the low temperature magnetic penetration depth  $\lambda(T)$ ,  $T^3$  to  $T$  crossover in the NMR rate, and the  $\omega^3$  to  $\omega$  crossover in the low frequency  $B_{1g}$  Raman response. Simple theories based on nearly-resonant scattering in the impurity  $T$ -matrix approximation (“dirty”  $d$ -wave) have accounted for these behaviors seen in materials of various quality and impurity dopings.

However, several inconsistencies arise when attempting to put together a complete picture. First, the magnitude of the impurity scattering needed to fit  $\lambda(T)$  and the extrapolated  $T = 0$  resistivity are generally much smaller than those needed to fit the measured frequency dependence of the infrared conductivity (IR) and the Raman response. In particular, the impurity scattering rate  $1/\tau_{imp} = 2\Gamma$  needed to fit the IR on high quality Y-123 was 100 times larger than that needed to fit microwave measurements [2], while values of  $\Gamma/\Delta_0$  ranging up to 0.5 were needed to interpret the Raman data taken on Bi-2201 [3], and some samples of Tl-2201 [4] and Hg-1223 [5]. Second, the “universal” dc conductivity  $\sigma(\omega \rightarrow 0, T = 0) = (e^2/2\pi\hbar)\xi/a$  [6] has not been convincingly observed and the low temperature variation of the conductivity  $\delta\sigma(T)$  changes slower than  $T^2$  [7]. Third, the transition temperature  $T_c$  is only moderately reduced by planar impurities compared to Abrikosov-Gorkov theory [8] (by about a factor of two to three). Lastly, the residual resistivity obtained for Zn doped Y-123 suggests that a strong contribution is present in  $d$ -wave scattering channels [9].

These inconsistencies reveal that the usual treatment of point-like  $s$ -wave impurities in a  $T$ -matrix approach may be too naive and neglects electronic correlations. Experimental evidence from transport measurements in Zn doped YBCO have revealed that the a single impurity embedded in the  $\text{CuO}_2$  plane disturbs the local en-

vironment and yields an effective scattering cross section diameter of  $\text{Zn}^{2+}$  of  $4.2\text{\AA}$  [10] and is thus extended. Theoretical studies have shown that static vacancies in a Heisenberg antiferromagnet enhance the staggered magnetic moment within a few lattice spacings around the vacancy [11], while studies of models with only short range antiferromagnetic (AF) correlations have shown that correlations dynamically generate finite-range impurity potentials from single site impurities [12].

In this paper we explore the role extended impurities have on transport properties in an attempt to resolve the abovementioned discrepancies. In particular, we re-examine the IR and the electronic Raman response of Bi-2212 including the effects of electronic correlations on both inelastic and elastic scattering potentials, and compare our results with the extrapolated  $T = 0$  normal state resistivity and the crossover temperature for  $\lambda(T)$ . We find that a consistent picture emerges when we include the extended range of impurity scattering as well as AF spin fluctuations.

Currently, knowledge of a  $T$ -matrix formulation for disorder in correlated systems is limited and generally approximate methods have been used [13]. Formally, one would need to include not only bare impurity and interaction self energies responsible for elastic and inelastic scattering, respectively, but also one must include terms in which mix elastic and inelastic potentials. In this way, a purely static bare impurity interaction changes in nature (can become dynamic) due to the inclusion of many-body effects. Ziegler *et al.* in Ref. [13] discussed how a point-like  $s$ -wave bare impurity potential can become extended due to the background of the correlated host. One can then proceed to calculate the  $T$ -matrix by using a *renormalized* Hamiltonian which describes the impurity potential in the correlated host.

Our starting point is the model Hamiltonian considered in Ref. [14], which represents the effects of impurities in a metal with short range AF order on a square lattice:

$$H_i = \sum_{\{1\},\sigma,\delta} \left[ \frac{V_0}{4} n_{1,\sigma} + t_I (c_{1,\sigma}^\dagger c_{1+\delta,\sigma} + h.c.) + V_1 n_{1+\delta,\sigma} \right].$$

The parameters  $V_0$  and  $V_1$  denote the on-site and extended impurity potentials, and  $t_I$  denotes the effect of impurities on the electron hopping to the impurity site. Focusing on a two parameter model using the specific relation  $V_1 = \alpha^2 V_0/4$  and  $t_I = \alpha V_0/4$ , an analytic solution for the single impurity  $T$ -matrix was obtained.  $\alpha$  is the control parameter which distinguishes between point-like ( $\alpha = 0$ ) and extended ( $\alpha \neq 0$ ) impurity potentials.

The algebraic solution for the impurity  $T$ -matrix is presented in Ref. [14], where the reader is referred to for details. In essence, the extended structure of the impurity potential requires a  $4 \times 4$  matrix formulation with respect to  $s$ ,  $p$ , and  $d$  scattering channels expressed in terms of the  $\mathbf{k}$  dependent basis functions of the square lattice. The impurity averaged self energy is determined via  $\hat{\Sigma}_i^{imp}(\mathbf{k}, i\omega) = n_i \hat{T}_{\mathbf{k}, \mathbf{k}}(i\omega)$ , with  $n_i$  the impurity concentration. The self energy can be expanded in Pauli matrices  $\hat{\Sigma}^{imp} = \sum_{i=0,3} \hat{\tau}_i \Sigma_i^{imp}$ , with the coefficients

$$\begin{aligned} \Sigma_0^{imp}(\mathbf{k}, i\omega) &= \frac{n_i V_0}{\delta^2 - \beta^2} \left\{ -(1 + \alpha \gamma_{\mathbf{k}})^2 (d_0 \beta + d_3 \delta) + \right. & (1) \\ & \left. (\alpha \gamma_{\mathbf{k}}^d)^2 (s_0 \beta - s_3 \delta) \right\} - \frac{n_i V_0 p_3 \alpha^2 ([\gamma_{\mathbf{k}}^{p_1}]^2 + [\gamma_{\mathbf{k}}^{p_2}]^2)}{p_0^2 - p_3^2 + a^{-2}}, \\ \Sigma_1^{imp}(\mathbf{k}, i\omega) &= \gamma_{\mathbf{k}}^d 2 \alpha n_i V_0 \left\{ \frac{(1 + \alpha \gamma_{\mathbf{k}}) a^+ \delta}{\delta^2 - \beta^2} + \frac{\alpha \gamma_{\mathbf{k}} a^-}{p_0^2 - p_3^2 + a^2} \right\}, \\ \Sigma_3^{imp}(\mathbf{k}, i\omega) &= \frac{n_i V_0}{\delta^2 - \beta^2} \left\{ (1 + \alpha \gamma_{\mathbf{k}})^2 (d_0 \delta + d_3 \beta) + \right. \\ & \left. (\alpha \gamma_{\mathbf{k}}^d)^2 (s_0 \delta - s_3 \beta) \right\} + \frac{n_i V_0 p_0 \alpha^2 ([\gamma_{\mathbf{k}}^{p_1}]^2 + [\gamma_{\mathbf{k}}^{p_2}]^2)}{p_0^2 - p_3^2 + a^{-2}}, \end{aligned}$$

and  $\Sigma_2^{imp}(\mathbf{k}, i\omega) = 0$ . Here  $s_{0,3}, d_{0,3}, p_{0,3}, \delta, \beta$  and  $a^\pm$  are constants [15] given by Eqs. (8-11) of Ref. [14]. The  $\mathbf{k}$ -dependent basis functions for a square lattice are  $\gamma_{\mathbf{k}}, \gamma_{\mathbf{k}}^d = [\cos(k_x a) \pm \cos(k_y a)]/2$ , and  $\gamma_{\mathbf{k}}^{p_1}, \gamma_{\mathbf{k}}^{p_2} = [\sin(k_x a) \pm \sin(k_y a)]/2$ . In the limit of  $\alpha \rightarrow 0$ , the  $T$ -matrix becomes momentum independent and recovers the well known results [16].

In the self consistent  $T$ -matrix approximation, the non-interacting Green's function is used to calculate the self energy and then the new Green's function is put back into the self energy calculation. The process is iterated until convergence is realized, which occurs typically after only a few iterations. We assume a strong on-site impurity interaction  $V_0 = 8t$ , take  $\epsilon_{\mathbf{k}} = -2t[\cos(k_x a) + \cos(k_y a)] + 4t' \cos(k_x a) \cos(k_y a) - \mu$ ,  $\Delta_{\mathbf{k}}(T) = \Delta_0(T)[\cos(k_x a) - \cos(k_y a)]/2$ , a weak coupling form for  $\Delta_0(T)$  and choose  $\Delta_0(T=0) = 4T_c = 0.4t$ . Here and throughout, lattice sizes of  $32 \times 32$  up to  $256 \times 256$  and typically over 1000 frequencies were used. Our results showed little size effects above the  $128 \times 128$  mesh. The chemical potential  $\mu$  was adjusted so that the filling  $\langle n \rangle = 0.825$ .

In the absence of vertex corrections, the homogeneous Raman response and the real part of the conductivity are

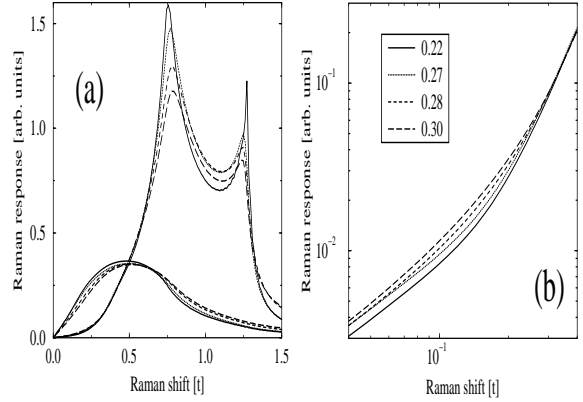


FIG. 1. (a)  $B_{1g}$  (upper set) and  $B_{2g}$  (lower) Raman response for  $T = 0.2T_c, \bar{U} = 0$  and 1% impurities. Here and in (b) the solid (dotted, dashed, long-dashed) line corresponds to  $\alpha = 0(0.5, 0.75, 1)$ . (b) Log-log plot of the low frequency  $B_{1g}$  Raman response determining the crossover frequency  $\omega^*$ . The legend gives the values of  $\omega^*/t$ .

$$\begin{aligned} \chi''_{\gamma, \gamma}(\mathbf{q} = \mathbf{0}, \Omega) &= \sum_{\mathbf{k}} \frac{\gamma_{\mathbf{k}}^2}{j_{\mathbf{k}}^{x^2}} \int \frac{d\omega}{N\pi} [f(\omega) - f(\omega + \Omega)] \\ \Omega \sigma'_{xx}(\mathbf{q} = \mathbf{0}, \Omega) &= \text{Tr} \left\{ \hat{\tau}_3 \hat{G}''(\mathbf{k}, \omega) \hat{\tau}_3 \hat{G}''(\mathbf{k}, \omega + \Omega) \right\}, \end{aligned} \quad (2)$$

where  $f$  is the Fermi function and the current vertex  $j_{\mathbf{k}}^x = e \partial \epsilon_{\mathbf{k}} / \partial k_x = 2tea \sin(k_x a) [1 - 2t'/t \cos(k_y a)]$ . The Raman response can be classified according to elements of the  $D^{4h}$  group:

$$\gamma_{\mathbf{k}}(\omega_I, \omega_S) = \begin{cases} b_{\omega_I, \omega_S} [\cos(k_x a) - \cos(k_y a)]/4, & B_{1g}, \\ b'_{\omega_I, \omega_S} \sin(k_x a) \sin(k_y a), & B_{2g}, \\ a_{\omega_I, \omega_S} [\cos(k_x a) + \cos(k_y a)]/4, & A_{1g}. \end{cases} \quad (3)$$

If the light scattering is non-resonant, the frequency dependence of the momentum independent prefactors  $b, b'$  and  $a$  can be safely neglected, and we can adjust these prefactors to account for overall intensity. It can be seen from the  $\mathbf{k}$ -dependence of the vertices that the  $B_{1g}$  response probes qp dynamics around the Brillouin Zone (BZ) axes,  $B_{2g}$  probes the diagonals, and  $A_{1g}$  is more of an average around the BZ and involves pure density fluctuations and backflow [17]. Higher order terms of increasingly more anisotropic basis functions could be considered but do not lead to appreciable differences except for the  $A_{1g}$  response (see Ref. [18] for details). From here on we only consider the  $B_{1g}$  and  $B_{2g}$  channels.

Results for the  $B_{1g}$  and  $B_{2g}$  response are plotted in Fig. (1a) for different values of  $\alpha$ . As seen in our previous studies of the DOS [14], turning on  $\alpha$  even slightly leads to an effective increase in the strength of the impurity potential. The increased impurity resonance at the Fermi level is manifest in the increasingly smeared spectra as well as the value of  $\omega^*$ , defined as the frequency where

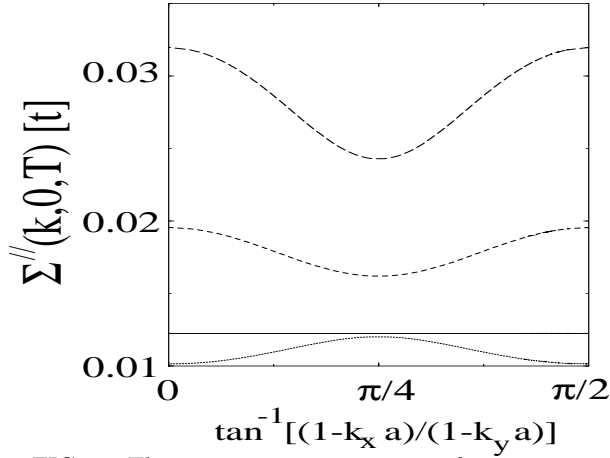


FIG. 2. The impurity scattering rate for momenta along the Fermi surface for  $\alpha = 0, 0.24, 0.48,$  and  $0.72$  (solid, dotted, dashed, long-dashed lines, respectively).

the cubic frequency dependence becomes sub-dominant [19], as shown in Fig. (1b). Since  $\alpha = 0.5$  corresponds to a nearest neighbor impurity potential  $V_1 = V_0/16$ , the presence of even a 6% nearest neighbor potential leads to a 23% increase in  $\omega^*$ . Therefore a much smaller concentration of extended impurities is needed to have the same effect as isotropic impurity scattering. The  $B_{2g}$  channel is only slightly affected by  $\alpha$ .

This is in accord with the impurity scattering being largest near the BZ axes in our model and only minorly dependent on  $\alpha$  near the BZ diagonals. This is seen in Fig. (2), which plots the normal state  $T = 0$  impurity scattering rate around the Fermi surface for different  $\alpha$ . Increasing  $\alpha$  from zero first decreases then increases the scattering rate near the BZ axes while only mildly affecting the rate along the BZ diagonals. Therefore we would expect the  $B_{1g}$  channel to be more sensitive than  $B_{2g}$  to the growth of scattering for increased  $\alpha$ .

As an important consequence, the IR (which has similar weighting to  $B_{2g}$ ) does not pick up regions where the scattering changes rapidly and is governed by small scattering along the BZ diagonals. The IR in the superconducting state is shown in Fig. (3) for different values of  $\alpha$  at a fixed impurity concentration. The IR does not appreciably change for  $\alpha$  up to 0.5. For larger  $\alpha$  spectral weight is shifted away from low frequencies as the scattering rate increases over the entire BZ [20], and a stronger shoulder near  $\Delta_{max}$  develops.

We now consider inelastic scattering in order to address the intensity observed at high frequencies. The origin of the flat background in IR and Raman at high frequencies has attracted a great deal of attention involving both Fermi liquid and non-Fermi liquid based theories. A correct approach would account not only for the featureless continuum but would be able to describe the polarization dependence of the Raman cross section and the differences between IR and Raman. Raman has shown strong evidence of two-magnon features in the insulating as well

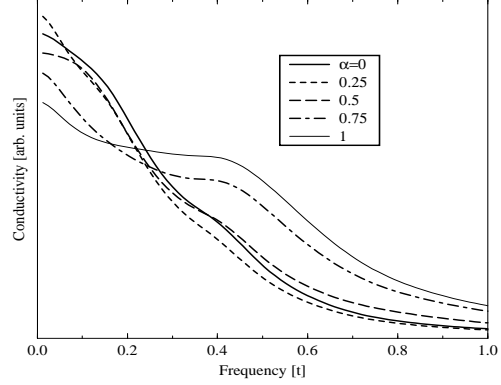


FIG. 3. The calculated IR at  $T=0.2T_c$ ,  $U = 0$ , and 2% impurities for  $\alpha = 0, 0.25, 0.5, 0.75$  and 1 (solid, dashed, long-dashed, dash-dotted lines, and thin solid lines, respectively).

as superconducting state, implying the role of spin fluctuations as a source for inelastic scattering [21]. The way in which spin fluctuations are included in calculating dynamic quantities has also attracted a large amount of attention. The main problem has been the degree in which strong local electron correlations are included and represented. Effective Hamiltonian [22] approaches based on Bragg-like scattering of quasiparticles for momentum  $\mathbf{Q} = (\pi, \pi)$  have been successfully employed to calculate various dynamic correlation functions, including IR [23] and Raman [24]. However, to a certain extent these approaches have their limitation as they do not adequately capture the strong multi-magnon scattering process required to approach the insulating phase from the metallic side [25].

Since here we are interested in only the low frequency behavior of the IR and Raman response, the details of the dynamic scattering are not crucial in that they only affect the response functions at larger frequencies. Therefore we take a simple route and include spin fluctuations in RPA,

$$V(\mathbf{q}, i\Omega) = \frac{3}{2} \frac{\bar{U}^2 \chi_0(\mathbf{q}, i\Omega)}{1 - \bar{U} \chi_0(\mathbf{q}, i\Omega)}, \quad (4)$$

where  $\bar{U}$  is a phenomenological parameter [we choose  $\bar{U} = 2t$ ].  $\chi_0(\mathbf{q}, i\Omega)$  is the non-interacting spin susceptibility,

$$\chi_0(\mathbf{q}, i\Omega) = \sum_{\mathbf{k}} \left\{ \frac{a_{\mathbf{k}, \mathbf{k}+\mathbf{q}}^+}{2N} \frac{f(E_{\mathbf{k}+\mathbf{q}}) - f(E_{\mathbf{k}})}{i\Omega - (E_{\mathbf{k}+\mathbf{q}} - E_{\mathbf{k}})} + \frac{a_{\mathbf{k}, \mathbf{k}+\mathbf{q}}^-}{4N} \right. \\ \left. \times \left[ \frac{1 - f(E_{\mathbf{k}+\mathbf{q}}) - f(E_{\mathbf{k}})}{i\Omega + E_{\mathbf{k}+\mathbf{q}} + E_{\mathbf{k}}} - \frac{1 - f(E_{\mathbf{k}+\mathbf{q}}) - f(E_{\mathbf{k}})}{i\Omega - E_{\mathbf{k}+\mathbf{q}} - E_{\mathbf{k}}} \right] \right\}. \quad (5)$$

Here  $E_{\mathbf{k}}^2 = \epsilon_{\mathbf{k}}^2 + \Delta_{\mathbf{k}}^2$  and the coherence factors are  $a_{\mathbf{k}, \mathbf{k}+\mathbf{q}}^{\pm} = 1 \pm \frac{\epsilon_{\mathbf{k}+\mathbf{q}} \epsilon_{\mathbf{k}} + \Delta_{\mathbf{k}} \Delta_{\mathbf{k}+\mathbf{q}}}{E_{\mathbf{k}+\mathbf{q}} E_{\mathbf{k}}}$ . This yields a self energy

$$\hat{\Sigma}^{\bar{U}}(\mathbf{k}, i\omega) = - \int \frac{dx}{\pi N} \sum_{\mathbf{q}} V''(\mathbf{q}, x) \frac{1}{2E_{\mathbf{k}-\mathbf{q}}}$$

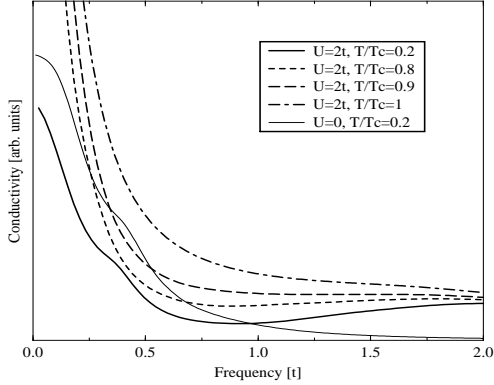


FIG. 4. The IR Conductivity for  $T = 0.2, 0.8, 0.9$ , and  $T_c$  (solid, dashed, long-dashed, dash-dotted lines, respectively) for 2% impurities and  $\alpha = 0.5$  and  $U = 2t$ . The thin solid line is for  $U = 0, T = 0.2T_c$  for comparison.

$$\left[ \frac{E_{\mathbf{k}-\mathbf{q}}\hat{\tau}_0 + \epsilon_{\mathbf{k}-\mathbf{q}}\hat{\tau}_3 + \Delta_{\mathbf{k}-\mathbf{q}}\hat{\tau}_1}{E_{\mathbf{k}-\mathbf{q}} + x - i\omega} [n(x) + f(-E_{\mathbf{k}-\mathbf{q}})] - \frac{-E_{\mathbf{k}-\mathbf{q}}\hat{\tau}_0 + \epsilon_{\mathbf{k}-\mathbf{q}}\hat{\tau}_3 + \Delta_{\mathbf{k}-\mathbf{q}}\hat{\tau}_1}{-E_{\mathbf{k}-\mathbf{q}} + x - i\omega} [n(x) + f(E_{\mathbf{k}-\mathbf{q}})] \right]. \quad (6)$$

The convolution of momentum sums in Eq. 6 is solved numerically via Fast Fourier Transform, where we keep the full  $\mathbf{k}$ -dependence and the real and imaginary parts of the self energy. We found that neglecting the real parts of the self energy and/or restricting momentum sums around the FS leads to a substantially smaller conductivity and misses a renormalization of the conductivity peak to frequencies slightly away from  $4\Delta$  in the superconducting state [2]. Combining both  $\hat{\Sigma}^{imp, \bar{U}}$ , the results for the IR and the Raman response for the  $B_{1g}$  and  $B_{2g}$  channels are summarized in Figs. (4) and (5). For both quantities the spin fluctuations yield a flat continuum at high frequencies in common with experiments and various different theories which yield a linear frequency dependence of the imaginary part of the self energy. The temperature dependence there is minimal and all the spectra converge to similar values by roughly  $\Omega \sim 2t$ . As the temperature is lowered, the low frequency IR falls in magnitude and develops a shoulder at  $\sim \Delta_{max}$  and a weak peak at  $\sim 4\Delta_{max}$ , while the spectral weight in the  $B_{1g}$  and  $B_{2g}$  channels reorganize from low frequencies to higher frequencies at  $\sim 2\Delta_{max}$  and  $0.65\Delta_{max}$ , respectively. Strong peaks associated with pair breaking and the van Hove structure ( $\sim t$ ) appear in the  $B_{1g}$  channel and become less pronounced as the temperature is increased due to the growth of spin fluctuation scattering. We note that at present there is no experimental indication of a peak in the  $B_{1g}$  which could be associated with a van Hove feature [3]. In our calculations further smearing of the van Hove peak is expected if dispersion is added in the  $c$ -direction or if stronger interactions are used which produce larger inelastic scattering at large frequencies.

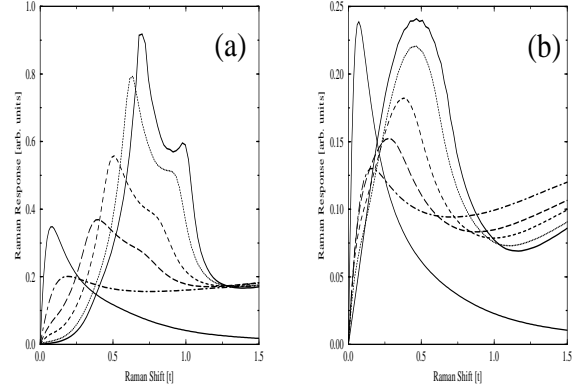


FIG. 5. Raman response for the  $B_{1g}$  (a) and  $B_{2g}$  (b) channel for  $\bar{U} = 2t, V_0 = 8t$ , 2% impurities, and  $\alpha = 0.5$  for  $T/T_c = 0.2, 0.6, 0.8, 0.9, 1$  plotted as the thick solid, dotted, dashed, long-dashed, and dotted-dashed lines. The thin solid line shows the response at  $T = T_c$  for  $\bar{U} = 0$  for comparison.

Moreover, a more correct multi-magnon approach would also wash out structure at higher frequencies.

Fits to the Raman spectra measured in the superconducting state at  $T = 0.5T_c$  of an as-grown sample of Bi-2212 are presented in Fig. 6, while fits to the IR in both the normal and superconducting state on a similar sample with a slightly higher  $T_c$  by taken by N. L. Wang *et al.* [26] are shown in Fig. 7. Here we have taken the parameters used in Fig. 5, have adjusted the prefactors  $b/b' = 1.46$  to account for the relative Raman intensities. For the IR, we use the  $c$ -axis lattice spacing of  $30\text{\AA}$  for Bi-2212 containing 2  $\text{CuO}_2$  bilayers to convert the 2D IR to 3D. We find that theory underestimates the IR scale by only a factor of 1.5 (the fits in Fig. 7 are scaled by this factor). We used slightly different values of  $t$  for Raman (81meV) than IR (69 meV), but equally good fits are obtained if we used different values for  $\Delta$ . The results agree exceptionally well with the measured spectra especially at low frequencies where the effects of impurities are dominant. The agreement lessens to only a qualitative level for  $\Omega > 1000 \text{ cm}^{-1}$  due to the small degree of spin fluctuations included (in RPA) and points to an inadequate description of the normal state.

Finally, we consider how the fitting parameters compare to transport data. Assuming a Drude model for  $\rho(T = 0) (\approx 10\mu\Omega\text{-cm})$  and a plasma frequency of 1.2 eV [27] implies a scattering rate  $1/\tau_{imp} = 15\text{cm}^{-1}$ , while the penetration depth  $T$  to  $T^2$  crossover [28] measured in the same sample [29] as the Raman data gives  $12 \text{ cm}^{-1}$ . Previous Raman fits using isotropic impurity scattering only and a Fermi surface restricted approach required  $1/\tau_{imp} = 2\Gamma = 72 \text{ cm}^{-1}$  [19]. Our calculation for  $\alpha = 0.5$  yields  $1/\tau_{imp}^{ave} = 23$  and  $20 \text{ cm}^{-1}$  for the FS averaged impurity scattering rate for the  $t = 81$  and  $69 \text{ meV}$ , respectively. Given the uncertainty in estimating  $\rho(T = 0)$  and  $\omega_{pl}$ , this is in favorable agreement with existing mea-

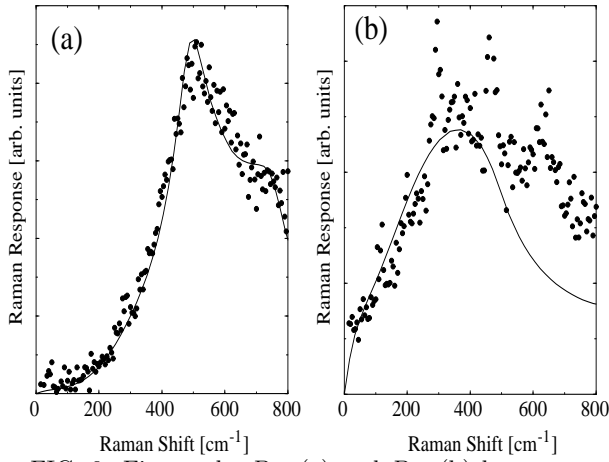


FIG. 6. Fits to the  $B_{1g}$  (a) and  $B_{2g}$  (b) low temperature spectra on Bi-2212 ( $T_c=86K$ ) taken by R. Hackl *et al.* in [3].

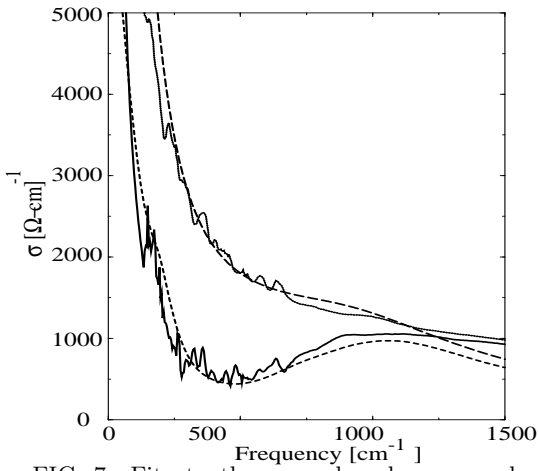


FIG. 7. Fits to the normal and superconducting IR on Bi-2212 ( $T_c=93K$ ) taken by N. L. Wang *et al.* [26].

surements.

In summary we have shown how the inclusion of electron correlations in both inelastic and elastic scattering potentials lead to a consistent description of the channel dependent Raman and IR response and lead to better fits than previously achieved. The overall intensity of the IR can be accounted for and the effect of extended impurities on the low frequency behavior of the Raman response can resolve the discrepancy between large impurity scattering rates needed previously for IR and Raman fits and the small rates needed for transport.

## ACKNOWLEDGMENTS

Acknowledgment (T.P.D.) is made to the Donors of the Petroleum Research Fund, administered by the American Chemical Society, for partial support of this research. We have benefitted from discussions with J. C. Irwin and R. Hackl, and we thank R. Hackl and N. L. Wang for sharing the data presented in Figs. 6 and 7, respectively.

\* Present address: Dept. of Physics, University of Waterloo, Waterloo, ON N2L 3G1, Canada.

- [1] J. Annett, N. Goldenfeld, and A. J. Leggett, *Physical Properties of High Temperature Superconductors*, Vol. 5, D.M. Ginsberg (Ed.), World Scientific, Singapore, 1996.
- [2] S. M. Quinlan, P. J. Hirschfeld, and D. J. Scalapino, *Phys. Rev. B* **53**, 8575 (1996).
- [3] D. Einzel and R. Hackl, *J. Raman Spect.* **27**, 307 (1996).
- [4] R. Nemetschek, O. V. Misochko, B. Stadlober, and R. Hackl, *Phys. Rev B* **47**, 3450 (1993).
- [5] A. Sacuto, R. Combescot, N. Bontemps, C. A. Müller, V. Viallet, and D. Colson, *Phys. Rev. B* **58**, 11721 (1998).
- [6] P. A. Lee, *Phys. Rev. Lett.* **71**, 1887 (1993).
- [7] S.Hensen, G. Müller, C. T. Rieck, and K. Scharnberg, *Phys. Rev. B* **56**, 6237 (1997); A. Hosseini, R. Harris, S. Kamal, P. Dosanjh, J. Preston, R. Liang, W. N. Hardy, and D. A. Bonn, *Phys. Rev. B* **60**, 1349 (1999).
- [8] R. J. Radtke, K. Levin, H.-B. Schüttler, and M. R. Norman, *Phys. Rev. B* **48**, 653 (1993); L. P. Gor'kov and P. A. Kalugin, *JETP Lett.* **41**, 252 (1985); P. Fulde, J. Keller, and G. Zwicknagl, in *Solid State Physics*, Vol. 41, F. Seitz, D. Turnbull, and H. Ehrenreich eds. (New York; Academic Press), 1988.
- [9] D. J. C. Walker, A. P. Mackenzie, and J. R. Cooper, *Phys. Rev. B* **51**, 15653 (1995).
- [10] T. R. Chien, Z. Z. Wang, and N. P. Ong, *Phys. Rev. Lett.* **67**, 2088 (1991).
- [11] N. Bulut, D. Hone, D. J. Scalapino, and E. Y. Loh, *Phys. Rev. Lett.* **62**, 2192 (1989).
- [12] D. Poilblanc, D. J. Scalapino, and W. Hanke, *Phys. Rev. Lett.* **72**, 884 (1994); A. V. Balatsky, M. I. Salkola, and A. Rosengren, *Phys. Rev. B* **51**, 15547 (1995); T. Xiang and J. M. Wheatley, *Phys. Rev. B* **51**, 11721 (1995).
- [13] W. Ziegler, D. Poilblanc, R. Preuss, W. Hanke, and D. J. Scalapino, *Phys. Rev. B* **53**, 8704 (1996).
- [14] A. P. Kampf and T. P. Devereaux, *Phys. Rev. B* **56**, 2360 (1997).
- [15] The constants  $s_i, d_i, p_i$  are the  $i$ -th Pauli matrix prefactor for the matrices  $\hat{s}, \hat{d}, \hat{p}$  in Eq. (8) of Ref. [14],  $a^\pm = a_2 \pm c_2$ , with  $a_2 = -\frac{V_0}{4N} \sum_{\mathbf{k}} 2\alpha\gamma_{\mathbf{k}}^d g_1$ ,  $c_2 = -\frac{V_0}{4N} \sum_{\mathbf{k}} (2\alpha\gamma_{\mathbf{k}}^d + \alpha^2[\cos(2k_x a) + \cos(2k_y a)]/2) g_1$ , and  $\delta \pm \beta = (s_0 \pm s_3)(d_0 \mp d_3) + a^{+2}$ .
- [16] P. J. Hirschfeld, P. Wölfle, and D. Einzel, *Phys. Rev. B* **37**, 83 (1988).
- [17] Note that the term “screening” has been used to describe the backflow. However, the backflow is independent of the charge of the carriers and comes into play solely from the pair interactions responsible for superconductivity. It yields the well known Anderson-Bogoliubov mode which restores gauge invariance. Details can be found in T. P. Devereaux and D. Einzel, *Phys. Rev. B* **51**, 16336 (1995).
- [18] T. P. Devereaux, A. Virosztek, and A. Zawadowski, *Phys. Rev. B* **54**, 12523 (1996).
- [19] T. P. Devereaux, *Phys. Rev. Lett* **74**, 4313 (1995); T. P. Devereaux and A. P. Kampf, *Int. J. Mod. Phys. B* **11**,

2093 (1997).

- [20] Vertex corrections must be included for finite  $\alpha$ . However, these corrections are proportional to  $\alpha^2$  and thus not important for small  $\alpha$ .
- [21] M. Rübhausen, O. A. Hammerstein, A. Bock, U. Merkt, C. T. Rieck, P. Guptasarma, D. G. Hinks, and M. V. Klein, Phys. Rev. Lett. **82**, 5349 (1999);
- [22] D. Pines, in *The Gap Symmetry and Fluctuations in High Temperature Superconductors*, J. Bok and G. Deutscher (eds.), Plenum Press, New York, p. 111 (1998).
- [23] D. Pines and B. Stojković, Phys. Rev. B **56**, 11931 (1997).
- [24] T. P. Devereaux and A. P. Kampf, Phys. Rev. B **59**, 6411 (1999).
- [25] J. R. Schrieffer, J. Low Temp. Phys. **99**, 397 (1995)
- [26] N. L. Wang, A. W. McConnell, B. P. Clayman, and G. D. Gu, Phys. Rev. B **59**, 576 (1999).
- [27] L. Forro, G. L. Carr, G. P. Williams, D. Mandrus, and L. Mihaly, Phys. Rev. Lett. **65**, 1941 (1990).
- [28] P. J. Hirschfeld and N. Goldenfeld, Phys. Rev. B **48**, 4219 (1993).
- [29] O. Waldmann, F. Steinmeyer, P. Müller, J. J. Neumeier, F. X. Régi, H. Savary, and J. Schneck, Phys. Rev. B **53**, 11825 (1996).